16th World Conference on Earthquake, 16WCEE 2017
Santiago Chile, January 9th to 13th 2017
Paper N° 1563
Registration Code: S-Z1461297123

Analytical Study on Simple Modeling for Lateral Resistance of Retaining Wall in Collision with a Base-Isolated Structure

T. Inubushi [(1)], Y. Miyamoto [(2)], T. Yamashita [(3)], T. Enomoto [(4)]

[(1)] *Japan, Dept. of Architecture and Building Engineering, Kanagawa University, inubushi@kanagawa-u.ac.jp*
[(2)] *Japan, Dept. of Architectural Engineering Division of Global Architecture, Osaka University,miyamoto@arch.eng.osaka-u.ac.jp*
[(3)] *Japan, Dynamic Control Design Office, tadamichi_yamashita-dcd@go6.fiberbit.net*
[(4)] *Japan, Dept. of Architecture and Building Engineering, Kanagawa University, enomot01@kanagawa-u.ac.jp*

Abstract

This paper uses 3D-FEM to estimate the response of a base-isolated structure when it collides uniformly and without twisting into a retaining wall, and proposes a method for simply modeling the lateral resistance of the retaining wall portion (retaining wall + backfill) in this situation. To summarize the proposed simple modeling method, the retaining wall is taken as a cantilever and the concept of dynamic interaction springs used in evaluating pile response is applied in order to represent the resistance of the backfill soil using springs and dashpots. A comparison of the simple modeling method with the 3D-FEM analysis showed that, despite slight differences in maximum response displacement and hysteresis loop shape, the lateral resistance characteristics corresponded well. This paper also conducted a collision analysis using the simple modeling method, and the results of this analysis also corresponded well with the 3D-FEM analysis results.

Keywords: Base-Isolated structure; Collision to retaining wall; 3D-FEM; Dynamic interaction; Simple modeling method

1. Introduction

There is concern that when seismic motion exceeding the design level is input into a base-isolated structure, the structure may collide with the retaining wall due to increased lateral deformation of the isolation layer. No actual cases of a base-isolated structure colliding with a retaining wall have been reported in past seismic observations in Japan, but research has been carried out examining the behavior of structures when colliding with retaining walls through small-scale model experiments and analytical studies using fiber models. Experiments involving full-scale base-isolated structure in collision with retaining walls are also being carried out, and trends in the behavior of structures when colliding with retaining walls are becoming clear [1].

However, there is still ambiguity surrounding the estimation of resistance characteristics of the retaining wall portion (retaining wall + backfill). Currently, there is no choice but to rely on dynamic analysis using FEM to accurately simulate collision phenomena, and this is extremely difficult in practical design.

Therefore, this paper aims to propose a method for simply modeling the lateral resistance of the retaining wall portion during a collision of a base-isolated structure into a retaining wall. First, we analyze the seismic response of a base-isolated structure–soil interaction system using 3D-FEM, and we estimate the structural behavior and impulse force when it collides uniformly and without twisting into the retaining wall. Next, we use the estimated impulse force to set the external force for estimating the lateral resistance of the retaining wall portion, and we confirm the load–deformation characteristics of the retaining wall portion through 3D-FEM analysis. Then, we propose the simple modeling method for estimating the lateral resistance of the retaining wall portion using fiber model, and compare the results of this method with the FEM analysis results. We also conduct collision analysis of the base-isolated structure using the simple modeling method, and we confirm the validity of the proposed method by comparing the structure response with the 3D-FEM analysis results.

2. 3D-FEM analysis model

Figure 1 shows the FEM analysis model. The soil is assumed to be a uniform sandy soil with Vs = 150 m/s, unit weight γ_t = 18.0 kN/m^3, Poisson's ratio ν = 0.40, and angle of internal friction φ=35°. The ground surface load is assumed to be 5.0 kN/m^2. The shear strength of the soil τ_f is given by the Mohr-Coulomb failure criterion shown in Equation (1). Here, c is cohesion, and in this paper, c = 0. σ_0 is the effective overburden pressure, and it is calculated using the soil's own weight and the ground surface load. The nonlinear characteristics of the soil are taken into account by approximating the hyperbolic model [2] to normal trilinear model.

$$\tau_f = c + \sigma_0 \cdot \tan\varphi \tag{1}$$

The structure is taken as a 10-story RC base-isolated building. The superstructure is modeled using shear springs in an elastic multi-degree-of-freedom system, and the seismic isolators are modeled using vertical springs and shear springs. Table 1 shows the specifications of the superstructure. Figure 2 shows the arrangement of the seismic isolators, and Tables 2 and 3 show the specifications of each isolator and the natural periods of the building. The vertical springs of the isolators are all taken to be elastic. The shear springs of the isolators are given elastic restoring force characteristics in the case of the natural rubber bearings, and normal bilinear restoring force characteristics for all other isolators. The depth of the girder directly above the isolation layer is taken as D = 1.5 m and the slab thickness as t_s = 0.2 m. The seismic isolation clearance is 0.5 m, and the base is a 2.0 m thick slab. The thickness of the retaining wall is taken as t = 0.3 m, and there are 10 divisions at 0.2 m intervals in the height direction of the retaining wall (Figure 3). The girder, slab, retaining wall, and base slab are all assumed to be elastic. The strength of the concrete used is taken as F_c = 36 N/mm^2, and the base slab is assumed to be rigid.

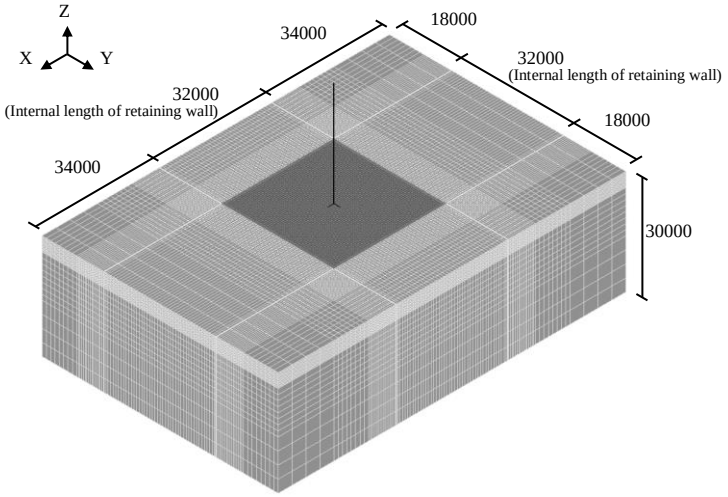

Fig.1 – 3D-FEM analysis model

Table 1 – Properties of superstructure

Story	Height (m)	Weight (kN)	Stiffness (kN/m)
10	3.0	1.361×10^4	2.958×10^6
9	3.0	1.297×10^4	3.366×10^6
8	3.0	1.297×10^4	3.501×10^6
7	3.0	1.297×10^4	3.538×10^6
6	3.0	1.297×10^4	3.688×10^6
5	3.0	1.297×10^4	3.772×10^6
4	3.0	1.297×10^4	3.976×10^6
3	3.0	1.322×10^4	4.331×10^6
2	3.0	1.322×10^4	4.584×10^6
1	3.0	1.322×10^4	6.584×10^6

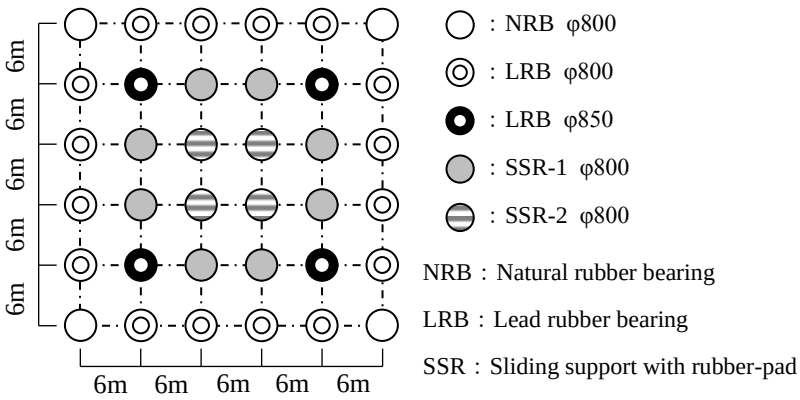

Fig.2 – Arrangement of isolators

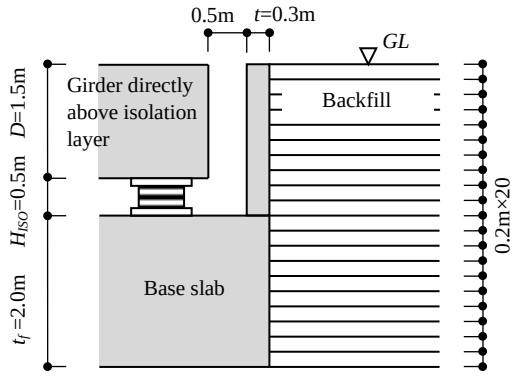

Fig.3 – Cross-section of retaining wall portion and isolation layer

Table 2 – Properties of isolators

Isolator	Diameter	Stiffness(kN/m)		Yield shear strength (kN)
		Initial	Secondary	
NRB	φ800	965	—	—
LRB	φ800	12961	997	203
	φ850	14495	1115	141
SSR-1	φ800	8436	8.4	66
SSR-2	φ800	8436	8.4	58

Table 3 – Natural period of structure

Mode	Isolation layer deformation		
	Zero(Fixed)	Small	500mm
1	0.735	1.433	4.350
2	0.256	0.397	0.428
3	0.158	0.210	0.213

3. 3D-FEM analysis model

The 3D-FEM model boundary conditions are assumed to be fixed at the bottom face and cyclic (equal displacement) at the sides. The structure is assumed to be supported by piles, and this restricts the vertical displacement of the underside of the base. Separation and sliding between the soil and the retaining wall or the underside of the base are not taken into account. Internal viscous damping is assumed to be Rayleigh damping, and for frequencies of 1 Hz and 10 Hz, in the structure system h = 2% (seismic isolator, h = 0%), and in the soil h = 1%. The input acceleration waveform is taken as that shown in Figure 4, and it is provided uniformly in X-direction of the bottom nodes.

Figure 5 shows the time history of relative displacement between the isolation layer and the retaining wall, and Figure 6 shows the time history of the response acceleration of the superstructure. For comparison purposes, each of the figures also shows the results when collision with the retaining wall was not considered. The displacement of the retaining wall is the response result at the top of the retaining wall in the center position of the width direction.

Figure 5 shows that the response displacement of the isolation layer increases from around 2.0 seconds, and collision between the base-isolated structure and the retaining wall occurs at around 2.55 seconds. The bottom edge of the girder directly above the isolation layer collides with the retaining wall, and then the base-isolated building behaves in contact with the retaining wall for approximately 0.12 seconds. In the non-collision analysis, the maximum response displacement of the isolation layer is approximately 543 mm. Figure 6 shows that the response acceleration of the superstructure increases rapidly after collision with the retaining wall, and the maximum response acceleration is 4.34 times that of non-collision for the 1st floor (directly above the isolation layer) and 4.72 times for the top floor.

Figure 7 shows the time-history waveform of impulse force when the base-isolated building collides with the retaining wall. The force is the nodal reaction force caused by contact between the building and the retaining wall, and Figure 7 shows the sum of the impulse force at nodes at GL -1.4 m, which is the position at which the maximum impulse force was obtained in the FEM analysis. When the base-isolated structure is not in contact with the retaining wall, the impulse force is 0, and so Figure 7 only shows the impulse force around the time of collision. Figure 7 shows that the peak impulse force occurs approximately 0.04 seconds after the start of the collision. Also, the shear coefficient obtained by dividing the maximum impulse force on the retaining wall portion at GL -1.4 m by the structure total weight is approximately 0.23.

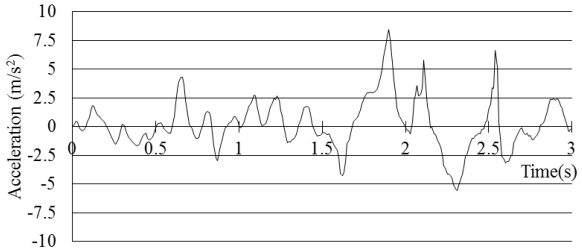

Fig. 4 – Input acceleration waveform

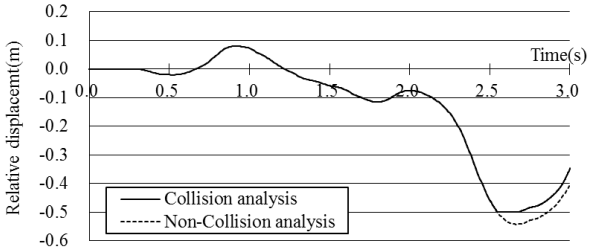

Fig. 5 – Time history of relative displacement between isolation layer and retaining wall

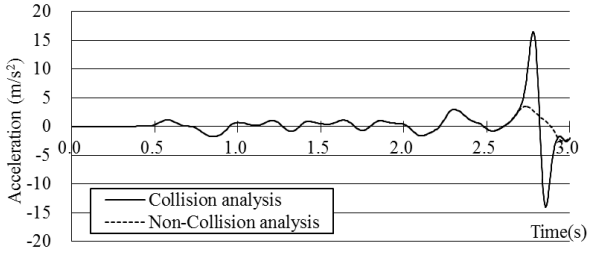

(a) Top floor

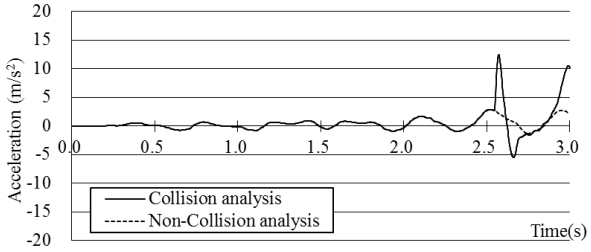

(b) 1st floor

Fig. 6 – Time history of structure response acceleration

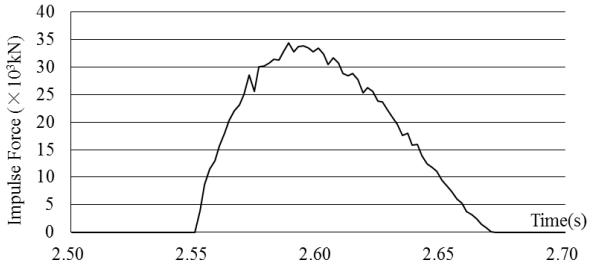

Fig. 7 – Time-history waveform of impulse force

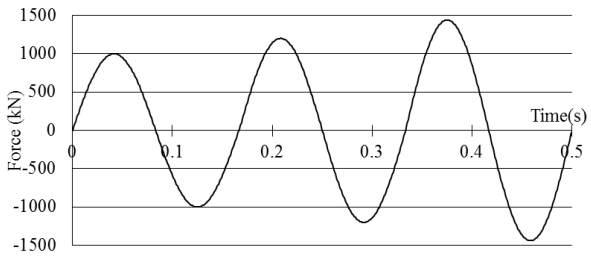

Fig. 8 – Excitation force

4. Estimation of lateral resistance of retaining wall portion

The lateral resistance of the retaining wall portion against the impulse forces obtained in the preceding section is estimated using a sine wave in which the interval from the start of collision to the peak impulse force is 1/4 wavelength. Here, the mean impulse force is defined as the force divided by the number of retaining wall nodes existing within the 30-m width of the structure (41 nodes). The lateral resistance of the retaining wall portion is examined using the FEM analysis model shown in Figure 1 with the structure system removed, except for the retaining wall and base. Figure 8 shows the waveform of the applied force. The maximum value of mean impulse force is normalized to 1,000 kN, and in order to confirm the hysteretic characteristics of the retaining wall portion, three sine waves of wavelength 0.167 seconds in which the maximum value of mean impulse force gradually increases by 1.2 times are applied to each retaining wall node existing within the width of the structure at each height. This section evaluates cases in which the force is applied at GL ±0 m (assuming a collision with the top part of the retaining wall) and at GL -1.4 m (assuming a collision with the bottom part of the retaining wall). As well as a retaining wall thickness of t = 0.3 m, a thickness of t = 0.2 m is also considered. Also, a cohesive soil backfill is considered in addition to a sandy soil backfill. Cohesive soil is assumed to range from GL ±0 m to GL -2.0 m, and sandy soil is assumed to exist at GL -2.0 m and deeper. Shear wave velocity V_s, unit weight γ_t, and Poisson's ratio v are taken to be the same as for the sandy soil. The cohesive soil's angle of internal friction is assumed to be φ = 0, cohesion c = 12.5 kN/m^2, and the ground surface load is taken as 0 kN/m^2. The results are given later.

5. Proposal of simple modeling method for lateral resistance of retaining wall portion

5.1 Procedure of simple modeling method

This section proposes a simple method for modeling the lateral resistance of a retaining wall portion using fiber model. To summarize, the retaining wall is taken as a cantilever, and the concept of dynamic interaction springs used in evaluating pile response is applied in order to represent the resistance of the backfill using springs and dashpots.

[Step 1]

Taking the retaining wall as a cantilever, a multi-degree-of-freedom bending-shear model is set.

[Step 2]

The dynamic interaction spring constant between the retaining wall and backfill per unit thickness k_{fsi} is found using Vesic's proposed equation (Equation (2a)) [3]. First, the retaining wall is divided into square sections with sides equal to the thickness of the retaining wall t, and the dynamic interaction spring per width t is calculated. Then, the dynamic interaction spring when the impact force acts linearly on the retaining wall k_{fsi} is found by multiplying by L/t. The dynamic interaction spring constant associated with each retaining wall node k'_{fsi} is found by taking the thickness of layer i as H_i and multiplying by the dominant thickness of the two layers adjacent to each node.

$$k_{fsi} = 0.65\frac{E_{si}}{1-v_{si}^{\ 2}}\left(\frac{E_{si}t^4}{E_cI_c}\right)^{1/12}\times\frac{L}{t}\ ,\ k'_{fsi} = \frac{1}{2}\left(k_{fsi-1}H_{i-1} + k_{fsi}H_i\right) \tag{2a,b}$$

[Symbols]

E_{si}: Young's modulus of soil in layer i v_{si} : Poisson's ratio of soil in layer i
E_c : Young's modulus of concrete I_c : Second moment of area per retaining wall length t
L : Length of retaining wall where collision is considered

The hyperbolic model [2] expressed by Equation (3) is assumed for the nonlinear characteristics given to the dynamic interaction spring.

$$P_i = k'_{fsi}\delta \Big/ \left(1+\frac{k'_{fsi}\delta}{P_{imax}}\right) \tag{3}$$

Here, δ is the displacement of the dynamic interaction spring, and P_{imax} is the ultimate subgrade reaction of the dynamic interaction spring. Rankine's passive earth pressure, expressed by Equation (4), is used for P_{imax}.

$$P_{imax} = \int_{z_2}^{z_1} (\gamma_{ti} z + w_0) K_{pi} dz \cdot L = \left\{ \frac{1}{2} \gamma_{ti} \left({z_1}^2 - {z_2}^2 \right) + w_0 (z_1 - z_2) \right\} tan^2 \left(\frac{\pi}{4} + \frac{\varphi_i}{2} \right) L \quad (4)$$

[Step 3]

The mass of the backfill is applied to the retaining wall nodes as an added mass ${}_{add}m_i$. The range of the backfill considered as added mass is taken as a cubic function distribution in the height direction based on the bending deformation of the cantilever (Figure 10). This 3t is determined from the displacement distribution on the surface of the backfill in the FEM analysis performed in the preceding section.

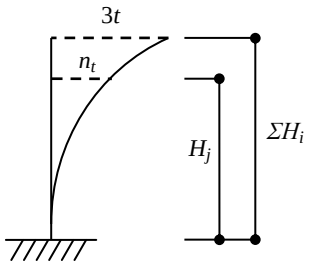

$$n_t = 3t \cdot \left(\frac{H_j}{H} \right)^3$$

$$_{add}m_i = n_t \cdot \frac{1}{2} \left(\frac{\gamma_i}{g} \cdot H_i + \frac{\gamma_{i-1}}{g} \cdot H_{i-1} \right) \cdot L$$

Fig. 10 – Distribution of added mass in height direction of retaining wall

[Step 4]

The time-history response displacement at each retaining wall node δ_i(t) is found by performing response analysis only once using an analysis model with the specifications found in Steps 1–3 (the analysis model shown later in Figure 13 with the dashpots removed).

[Step 5]

Assuming that the maximum shear strain of the backfill is equal to the maximum deformation angle of the retaining wall, the maximum response deformation angle of the retaining wall γ_{imax} is found by dividing the maximum relative displacement between each node $\Delta\delta_{imax}$ obtained in Step 4 by the distance between each node H_i. Then, the equivalent stiffness at maximum response of the backfill G_i' is found, and the equivalent S-wave velocity V'_{si} is found using G_i'.

$$\gamma_{imax} = \Delta\delta_{imax} / H_i \ , \ G_i' = \frac{\tau_{imax}}{\gamma_{imax}} \ , \ V'_{si} = \sqrt{G_i' / \rho_i} \quad (5a\text{-}c)$$

[Symbols]

ρ_i : Density of soil in layer i

[Step 6]

Using the equivalent S-wave velocity V'_{si}, a method devised by Gazetas et al. is applied to find the damping coefficient ${}_1c_{gsi}$ by Equations (6) [4]. Here, the direction of wave propagation is considered to be the soil side only, as shown in Figure 12.

$$V'_{Lai} = \frac{3.4 V'_{si}}{\pi (1 - \nu_{si})} \ , \ {}_1c_{gsi} = \rho_i t \cdot \frac{1}{2} V'_{Lai} \times \frac{L}{t} \quad (6a,b)$$

[Symbols]

V'_{Lai} : Lysmer's wave velocity in layer i $\left(= 3.4 V'_{si} / \pi (1 - \nu_{si}) \right)$

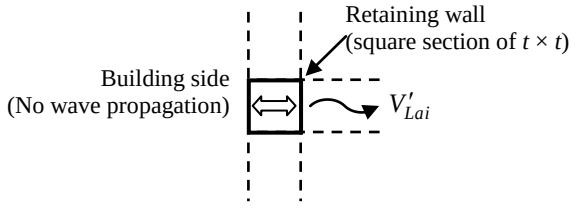

Fig. 12 – Direction of wave propagation

[Step 7]

The damping coefficient in the free field ${}_2c_{gsi}$ is also found in the same way as in Steps 5 and 6. However, in Step 5, maximum shear strain and Lysmer's wave velocity V_{Lai} are found from the time-history response displacement of each node in the free field. Then, the damping coefficient given to the dashpot per unit thickness c_{gsi} is found by Equation (7) and (8).

$$ {}_2c_{gsi} = \rho_i t \cdot \frac{1}{2} V_{Lai} \times \frac{L}{t} \tag{7} $$

$$ c_{gsi} = \alpha \cdot {}_1c_{gsi} + (1-\alpha)\, {}_2c_{gsi} \tag{8} $$

Here, it is assumed that α = 4/5. Also, the damping coefficient of the dashpot associated with each retaining wall node c'_{gsi} is calculated in a similar way to Equation (2b) by multiplying by the dominant thickness of the two layers adjacent to each node.

$$ c'_{gsi} = \frac{1}{2}\left(c_{gsi-1} \cdot H_{i-1} + c_{gsi} \cdot H_i\right) \tag{9} $$

The above procedure completes the analysis model (Figure 13) used in the simple modeling method. In this section, because the force is applied directly to the retaining wall portion, it is considered to have no effect on the free field, and the free field is assumed to be fixed (elastic state).

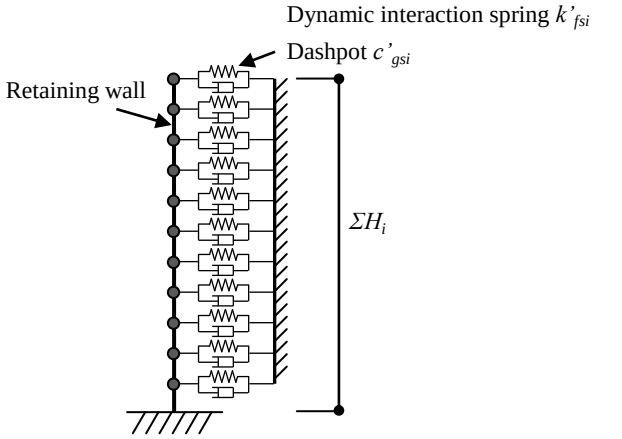

Fig.13 – Analysis model used in simple modeling method

5.2 Verification of simple modeling method

Using the analysis model in Figure 13 obtained from the procedure given in the preceding section, estimation is carried out of the lateral resistance of the retaining wall portion. The waveform and position of the applied force, and the retaining wall shape, are the same as in the FEM analysis. The mesh width of the FEM model (= 0.75 m) is used for the retaining wall width L, and the displacement at the center of the retaining wall in the width direction is used in calculating γ_{imax}.

Figures 14 and 15 show a comparison of the load–deformation relationship of the retaining wall portion obtained from the FEM analysis in the preceding section and from the simple modeling method when the backfill is sandy soil; and Figures 16 and 17 show the same for a backfill of cohesive soil.

The hysteresis loop of the retaining wall portion is spindle-shaped in each case, and it has high stiffness in the initial stages of force application. This is considered to be because the effect of the backfill, which is still in an elastic state, is relatively large, and this is particularly noticeable in the case of force application at GL ±0 m. There is good agreement between the simple modeling method and the FEM analysis with respect to initial stiffness. With respect to maximum deformation, when the backfill is sandy soil, the simple modeling method estimates it as slightly smaller than the FEM analysis results, and when the backfill is cohesive soil, it is slightly larger. The area of the hysteresis loop is smaller when the retaining wall thickness is t = 0.3 m compared to when it is t = 0.2 m. This is considered to be because, when t = 0.3 m, the retaining wall stiffness is high and so the backfill does not become very plastic, and also because the retaining wall response velocity is lower than when t = 0.2 m and so the effect of radiation damping is small. Also, a tendency for the area of the hysteresis loop during unloading to increase slightly as the position of force application approaches the base of the retaining wall can be identified in the simple modeling method compared to the FEM analysis. However, both methods show good agreement, and are capable of highly accurate estimations.

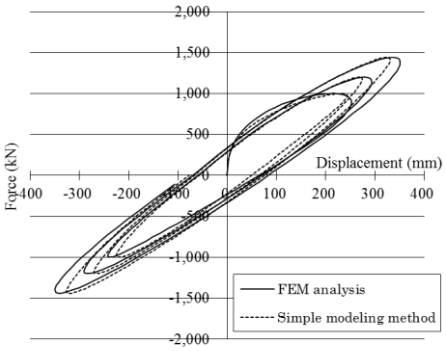

(a) Force applied at GL ± 0 m

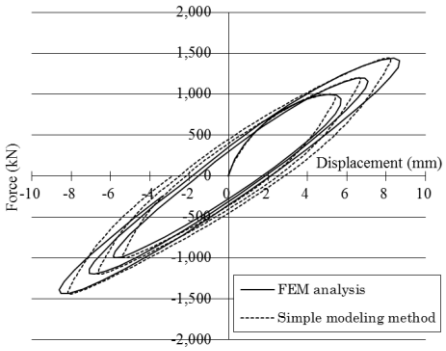

(b) Force applied at GL -1.4 m

Fig. 14 – Load–displacement relationship (sandy soil: retaining wall thickness t = 0.2 m)

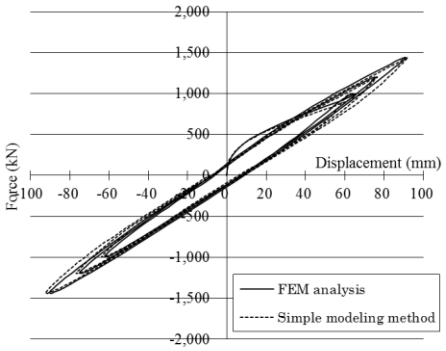

(a) Force applied at GL ± 0 m

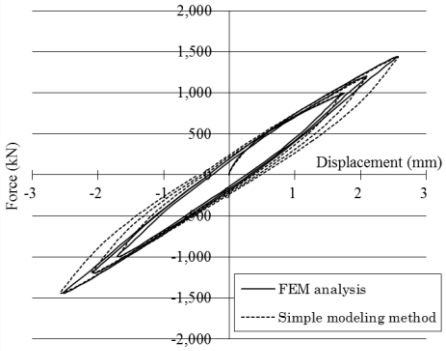

(b) Force applied at GL -1.4 m

Fig. 15 – Load–displacement relationship (sandy soil: retaining wall thickness t = 0.3m)

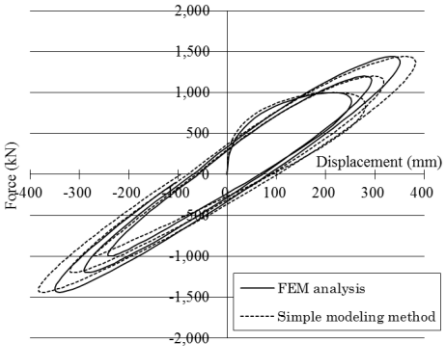

(a) Force applied at GL ± 0 m

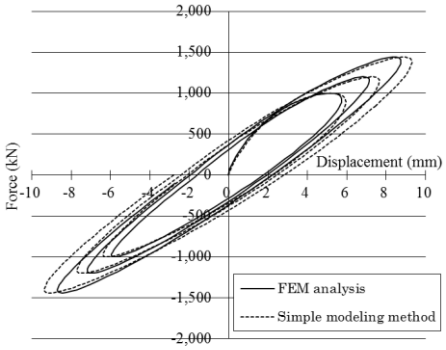

(b) Force applied at GL -1.4 m

Fig. 16 – Load–displacement relationship (cohesive soil: retaining wall thickness t = 0.2m)

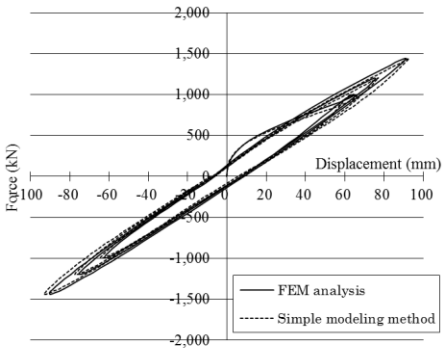

(a) Force applied at GL ± 0 m

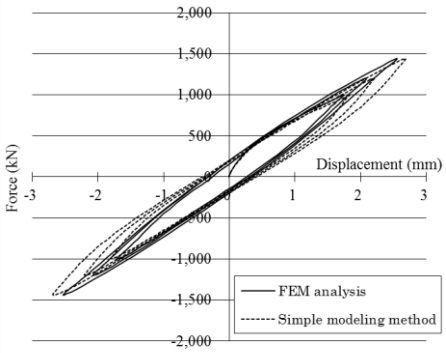

(b) Force applied at GL -1.4 m

Fig. 17 – Load–displacement relationship (cohesive soil: retaining wall thickness t = 0.3m)

6. Collision analysis using simple modeling method

6.1 Analysis model and analysis conditions

Using the model created from the simple modeling method for lateral resistance of a retaining wall portion, a collision analysis is carried out using time-history response analysis, and the results are compared with the FEM analysis results obtained in Section 3.

Figure 18 shows the collision analysis model using the simple modeling method. To reproduce the FEM analysis model shown in Figure 1, the free field and superstructure are modeled using shear springs in a multi-degree-of-freedom system. As described in the preceding section, the retaining wall is taken as beam element, and the free field and retaining wall are connected by dynamic interaction springs and dashpots represented by Equations (3) and (13). As described in Steps 4 and 5 in Section 5.1, the dashpot damping coefficient is found using the maximum response deformation angle of the retaining wall obtained by performing collision analysis only once using the analysis model shown in Figure 18 with the dashpots removed.

Directly below the superstructure, an element with the same height as the depth of the girder directly above the isolation layer is modeled. This is to take into account the height of the collision between the building and the retaining wall, and it is modeled as a rigid body on the assumption that the lateral shear stiffness of the girder is sufficiently large. Nodes are established in the rigid body at the same interval as in the retaining wall, and linear springs (hereafter, referred to as "collision springs") with a gap equal to the seismic isolation clearance are placed between each node of the rigid body and retaining wall (Figure 19). The stiffness of each collision spring is found by multiplying the sum of axial stiffness of the girder directly above the isolation layer perpendicular to the collision surface (Equation (10a)) by the ratio of dominant length of each rigid body node to girder depth (Equation (10b)).

$$K_i = \sum \frac{E_{c1} A_j}{B_j} \ , \ K_i' = \frac{1}{2}\left(K_i \frac{H_{i-1}}{D} + K_i \frac{H_i}{D} \right) \qquad (10a,b)$$

[Symbols]

E_{c1}: Young's modulus of concrete in girder directly above isolation layer

A_j, B_j: Axial cross-sectional area of girder directly above isolation layer perpendicular to collision surface at j, and girder length

D : Depth of girder directly above isolation layer

Here, because the depth of the girder directly above the isolation layer is D = 1.5 m, the collision springs are placed in the range of GL ±0 m – GL -1.4 m. Also, the seismic isolators are modeled as springs in the same way as in the FEM analysis, and they are placed in parallel directly below the rigid body.

The specifications assigned to each element and conditions such as internal viscous damping are the same as in the FEM analysis. Also, the length of the retaining wall at the collision surface L is taken as the building width, 30 m. Similar to the FEM analysis, the acceleration waveform shown in Figure 4 is input into the bottom free-field node. At the nodes directly below the isolation layer and at the base of the retaining wall, the input should be provided with the spring and dashpot that simulate the effect of dynamic interaction with the structure in connection with the free field; however, here, the response acceleration waveform at the center of the underside of the base obtained from the non-collision FEM analysis is input.

Figure 20(a) shows the restoring force characteristics of the entire isolation layer (isolation layer + collision springs) in the collision analysis using the simple modeling method; and Figure 20(b) shows a magnification of the area near response displacement 0.5 m in Figure 20(a), which is where the collision occurs. The shear force in each figure is the sum of the isolation layer response shear and impulse forces, and the displacement is the isolation layer's inter-story drift response. Comparing the restoring force characteristics of the entire isolation layer obtained from the FEM analysis and the simple modeling method, a difference of approximately 20% is found in the maximum response shear force and a difference of approximately 5 mm in the isolation layer response displacement at the time of collision. The simple modeling method largely captures the trends in the restoring force characteristics of the entire isolation layer from the FEM analysis. Figure 21 shows the time

history of response acceleration of the top of the superstructure and of the first floor. For comparison purposes, the results are shown together with the FEM analysis results from Section 3 and the results when the collision springs stiffness K_i' are set to a sufficiently large value, i.e. the axial stiffness of the girder directly above the isolation layer perpendicular to the collision surface is assumed to be sufficiently large (hereafter, referred to as the "rigid collision springs" case).

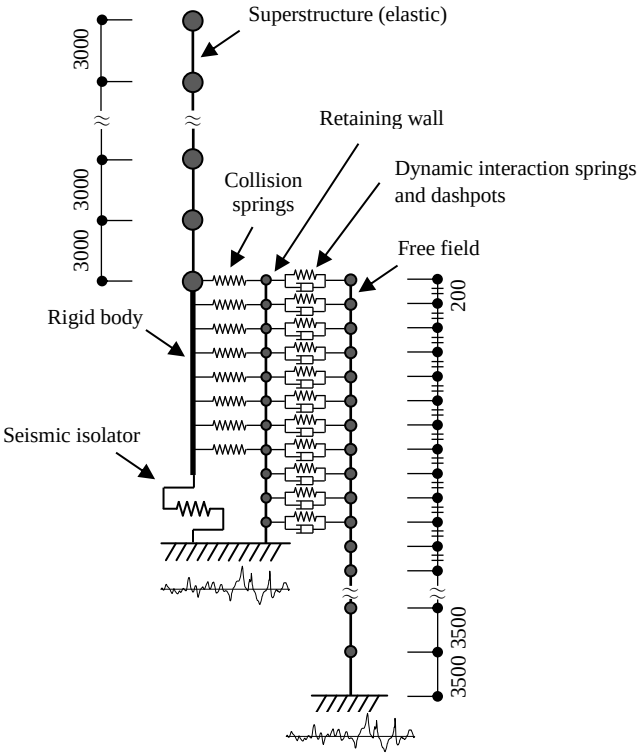

Fig. 18 – Collision analysis model using simple modeling method

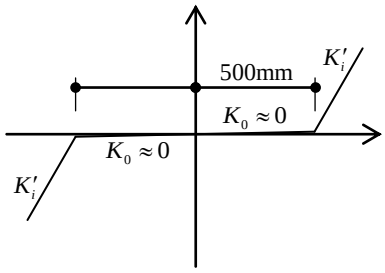

Fig. 19 – Collision spring

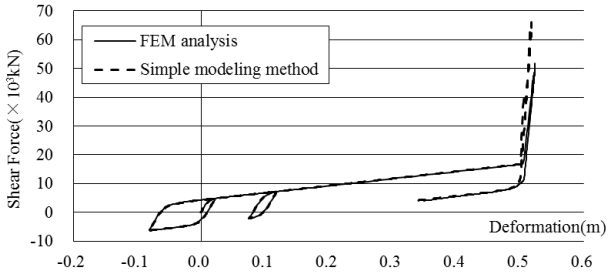

(a) Behavior of entire isolation layer

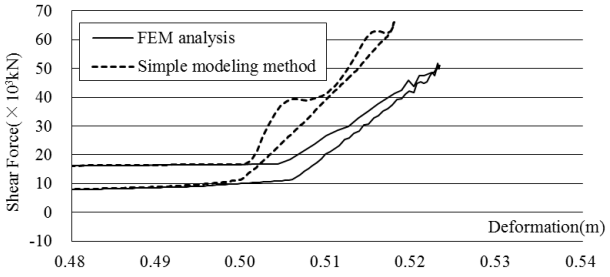

(b) Magnification of area near response deformation 0.5 m

Fig. 20– Restoring force characteristics of entire isolation layer in simple modeling method

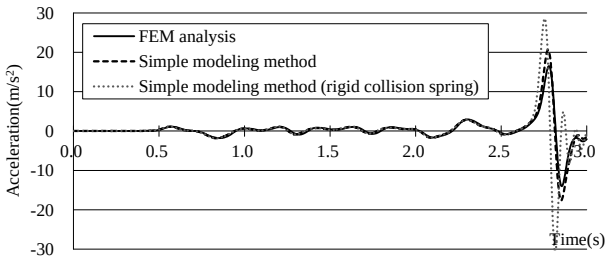

(a) Top floor

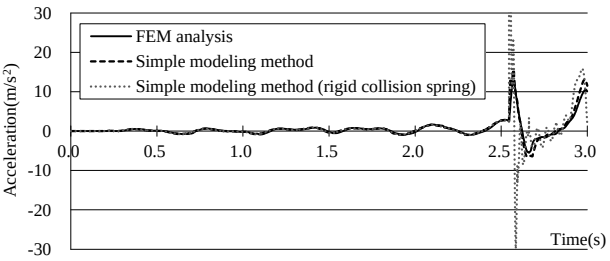

(b) 1st floor

Fig. 21 – Comparison of time history of structure response acceleration

In the time history of response acceleration in Figure 21 the maximum response acceleration is overestimated by approximately 20% using the simple modeling method, and that difference is slightly larger at the top floor compared to the first floor. However, the time-history waveform corresponds well with the FEM analysis results. Meanwhile, in the case of the rigid collision springs, there is a large difference in the maximum response value corresponding to approximately 1.5 times at the top floor and approximately 4 times at the first floor, compared to the case in which K_i' is set using Equation (10) taking into account axial stiffness of the girder directly above the isolation layer, and this shows that the estimation of collision springs stiffness are also a matter of importance.

7. Conclusion

The findings of this paper are summarized below.

1) The response acceleration of the building increased rapidly after collision with the retaining wall, and the maximum response acceleration was 4.34 times that of non-collision for the first floor and 4.72 times for the top floor. Also, the shear coefficient obtained by dividing the maximum impulse force on the retaining wall portion at GL -1.4 m by the building's total weight was approximately 0.23.

2) We proposed a simple modeling method for the estimation lateral resistance of a retaining wall portion using fiber model. A comparison of the load–displacement relationship of the retaining wall portion obtained from the simple modeling method and from the 3D-FEM analysis showed good agreement between both methods. Also, when retaining wall thickness t = 0.2 m, the area of the hysteresis loop was larger than when t = 0.3 m, and this showed that the backfill soil has large influence on the resistance characteristics of the retaining wall portion.

3) Comparing the collision response results from the simple modeling method and the FEM analysis showed that the simple modeling method successfully captured the trends in restoring force characteristics of the entire isolation layer obtained from the FEM analysis. The time histories of response acceleration and inter-story drift found using both methods corresponded well. The maximum response values were overestimated in the case of the rigid collision springs, and this showed the importance, not only of estimating the retaining wall portion, but also considering the axial stiffness of the girder directly above the isolation layer perpendicular to the collision surface.

8. References

[1] Goro Miwada, Takeshi Sano, Hideo Katsumata, Jumpei Komaki, Noriko Takiyama, Yoshihiro Onishi, Yasuhiro Hayashi: Experimental Study on Hysteresis Characteristics of the Retaining Wall of the Base-Isolated Building, Proceedings of the 15th World Conference on Earthquake Engineering (15WCEE, Lisbon), 2012.9

[2] Kondner, R. L.: Hyperbolic Stress-strain Response; Cohesive Soils, Proc. ASCE, SM1, pp.143-155, 1963

[3] Vesic, A. B.: Bending of Beams Resting on Isotropic Elastic Solid, J. Engrg. Div., ASCE, Vol.87, No.EM2, pp.35-53, 1961

[4] Gazatas, G. and Dobry, R.: Horizontal Response of Piles in Layered Soils, J. Geotech. Engrg. Div., ASCE, Vol.110, 20-40, 1984